Available online at www.sciencedirect.com
ScienceDirect
Physics Letters A 369 (2007) 323–327
PHYSICS LETTERS A
www.elsevier.com/locate/pla

Nanodomain shock wave in near-field laser–material interaction

Xuhui Feng, Xinwei Wang *

Department of Mechanical Engineering, N104 Walter Scott Engineering Center, The University of Nebraska-Lincoln, Lincoln, NE 68588-0656, USA

Received 8 March 2007; received in revised form 25 April 2007; accepted 30 April 2007

Available online 6 May 2007

Communicated by R. Wu

Abstract

In this work, molecular dynamics simulation is conducted to explore the shock wave phenomena in a nanodomain in near-field laser–material interaction. A large system consisting of over 800,000 atoms is studied. The work focuses on the kinetic and physical properties of the disturbed gas compression driven by the high speed movement of the molten particulates ejected from the solid target in a nanodomain. The quick interaction between solid and gas atoms compresses the gas and forms a steep shock wave front, which moves at a supersonic speed. The fast compression of gas also induces a steep interface of density, temperature and pressure distribution, which is viewed as typical characteristics of nanoscale shock waves. Evolutions of shock wave front position, velocity and Mach number are also explored and show quick decay during wave propagation.

PACS: 61.46.-w; 79.20.Ds; 52.65.Yy; 52.35.Tc

Keywords: Shock wave; Nanodomain; Near-field laser–material interaction; Molecular dynamics

1. Introduction

In the past decade, different near-field techniques, such as near-field scanning optical microscopy (NSOM) [1], superlens [2], nanoscale aperture [3,4], and scanning probe microscope (SPM) [5], have been developed to overcome the diffraction limit in laser-assisted manufacturing and material processing. In these near-field techniques, the laser beam can be focused to a small spot of tens of nanometers. Taking the laser-assisted STM as an example, the optical field can be enhanced by two orders of magnitude and focused to an extremely localized domain [6]. This enhanced optical field reaches the surface of the sample and causes chemical and physical changes of the material [7–16]. In laser-assisted nanomanufacturing, as a direct consequence of heating, the nanodomain of the sample under manufacturing experiences intense phase change, stress development and propagation. Because of the strong laser heating, the atoms right in the irradiated region will gain extraordinarily high kinetic energy and move out of the surface. This high-speed movement could compress ambient gas atoms in quite a short time, leading to a strong shock wave. The formation of the shock wave in the nanoscale domain could significantly affect the laser–material interacting zone and the nanostructuring process. In the past, very little research has been done to study laser-induced shock waves in nanoscale gas domains during near-field nanostructuring. According to work by Luo et al. [17], the interaction of laser irradiation with matter can induce inertially confined high-pressure plasma and vapor. In work by Kohen and Martens [18], a pump laser pulse excites impurity molecules embedded in a solid host to a repulsive electronic state, and then the resulting photofragments collide with neighboring host atoms and create a localized nanoscale shock wave through the lattice. Villagrán-Muniz et al. [19] have monitored the evolution of shock wave and thermal expansion of the hot air in the core of decaying plasma by using the probe beam deflection method. Jeong et al. [20] also used the probe beam deflection technique to measure the propagation of a shock wave and material vapor plume generated during excimer laser ablation of aluminum. Most of these works focused on the shock wave that happened in systems of one single medium, or

* Corresponding author. Tel.: +1 (402) 472 3089; fax: +1 (402) 472 1465.
E-mail address: xwang3@unl.edu (X. Wang).

0375-9601/$ – see front matter
doi:10.1016/j.physleta.2007.04.106

of large scale. Wang's previous work [21] has simulated laser-assisted nanomanufacturing, but no concern has been given to the environment in the event that it is not a vacuum. If the surrounding is filled with a gas, the nanoscale laser heating would produce a very high pressure, which then consequently induces a nanoscale shock wave in the ambient gas.

2. Methodologies for domain design and simulation

In order to fill the above knowledge gap, a modified system different from the models in our previous work is established to study nanoscale shock waves in near-field laser-assisted interaction. In this work, the simulated system includes two sub-domains. The first sub-domain is an argon thin film (target) positioned in the gas environment, and the lattice constant a for each face-centered-cubic (fcc) cell is 5.414 Å. This part is comprised of 5 fcc units (2.707 nm) in the x direction, 648 fcc units (350.83 nm) in the y direction and 60 fcc units (32.48 nm) in the z direction. For the gas domain, when referring to one gas unit for initial construction, the lattice constant is enlarged to 4 times argon lattice constant. In the z direction, the gas domain has 20 fcc units (43.31 nm) below the film and 100 fcc units (216.6 nm) above the film. Periodical boundary conditions are applied along the x, y, and z directions. A total of 855,360 atoms are simulated in this case.

The film material takes argon since its physical and chemical properties have been thoroughly studied. The gas material takes the same molecular mass as argon, but with a modified interatomic potential for the convenience of computation. For the model gas, only the repulsive force is considered between atoms. Except this, the model gas shares same parameters as the argon for MD simulation. In MD simulation for argon, the LJ well depth parameter ε and equilibrium separation σ take 1.653×10^{-21} J and 3.406 Å, respectively. The half-step leap-frog scheme is used [22] in this work with a time step of 25 fs. The interaction between atoms is neglected at a cutoff distance of 2.5σ. The enhanced near-field laser beam comes from the $-z$ direction and is assumed to have a distribution of

$$I = I_0 \cdot \exp\left(-(\vec{r} - \vec{r}_0)^2/r_g^2\right) \cdot \exp\left(-(t - t_0)^2/t_g^2\right), \quad (1)$$

where I_0 is a laser beam intensity constant, $\vec{r}_0$ is the center of the sample surface, $r_g = 5$ nm, $t_0 = 10$ ps, and $t_g = 3$ ps. An artificial absorption depth (τ) of 10 nm is employed in the simulation. When the laser beam goes through every cell along the z direction, the atoms in each cell absorb part of the energy with considering the exponential absorption of the laser beam in the incident direction. The absorption of laser in the sample is achieved by exciting the kinetic energy of atoms while keeping their momentum conserved. Details of the computational principles and laser energy absorption are described in our previous work [21,23]. The laser pulse has an energy of 0.75 fJ ($1\ \text{fJ} = 1 \times 10^{-15}$ J), which is corresponding to a maximal energy density level of 180 MW/cm^2.

Before applying laser heating, an equilibrium simulation is performed for 4000 steps (100 ps) to make the system achieve an expected temperature of 50 K. The equilibrium simulation is performed for the gas and solid (target) separately and simultaneously. After the equilibrium process, another 4000 steps simulation is performed to eliminate the disturbance introduced by the equilibrium procedure and to keep the system in minimal energy state. After these processes, the initial temperature of the whole region maintains at 50 K. In our simulation, because the distance between gas atoms is far beyond the interaction range (cutoff distance), this gas can be treated as ideal gas. According to the ideal gas law, the initial gas pressure is estimated to be 0.27 MPa. Our MD result shows that the initial gas pressure is 0.23 MPa, very close to this ideal gas estimation, confirming the ideal gas assumption. Under this condition, the sound speed is calculated to be 132 m/s.

3. Results and discussion

Fig. 1 presents the snapshots of atomic positions in the simulated domain at different times. In work by Porneala and Willis [24] for nanosecond laser ablation of aluminum, phase explosion and shock wave generation and propagation were observed directly. Although the simulation in this work differs from theirs in time and scales, we find that the shock wave generation and propagation shares the similar trend. The inset in Fig. 1 (200 ps) is from the work by Porneala and Willis [24] for comparison purpose. It can be clearly observed that at 50 ps, the explosion of the sample is very intense, and the solid atoms are moving out with a high speed. This sudden change rapidly compresses the adjacent gas region, causing a spherical interface made of compressed gas atoms. This means at the moment of 50 ps, a shock wave already forms. At 100 ps, the explosion has finished for a while, and the fast moving target atoms still keep propagating and compressing the ambient gas region. Therefore the spherical interface becomes much more evident. This shock wave moves very fast. In a period of 50 picoseconds, it moves about 25 nm, corresponding to an average velocity of about 500 m/s, much higher than the sound speed (132 m/s) in the ambient gas. In addition, according to the different colors shown in Fig. 1, the target atoms mix very little with the gas. When time reaches 200 ps, the thickness of the gas in the shock wave becomes larger. Due to the increase of the shock wave thickness and the slowdown of target atoms, the mixing of the two kinds of atoms is still weak. From the density distribution of the interface and mixed region, it can be concluded that the movements of target and gas atoms are primarily in the direction perpendicular to the sample surface. At 400 ps, the propagation of the shock wave still goes on, and its thickness gets even larger. Because of the decrease of shock wave velocity and temperature during propagation, the shock wave front is not so distinct as before. Appreciable mixing of gas and target atoms is observed. The speed of the shock wave front is still as high as 300 m/s.

For the shock wave, the physical properties (density, temperature, pressure, velocity) of the medium in it generally change sharply and significantly from the compressed region to the normal ambient gas. To confirm this feature of the shock wave in a nanodomain, Fig. 2 shows the distribution of density, temperature and pressure of the system in a y–z plane at 200 ps. In order to eliminate the statistical uncertainty, the local temper-

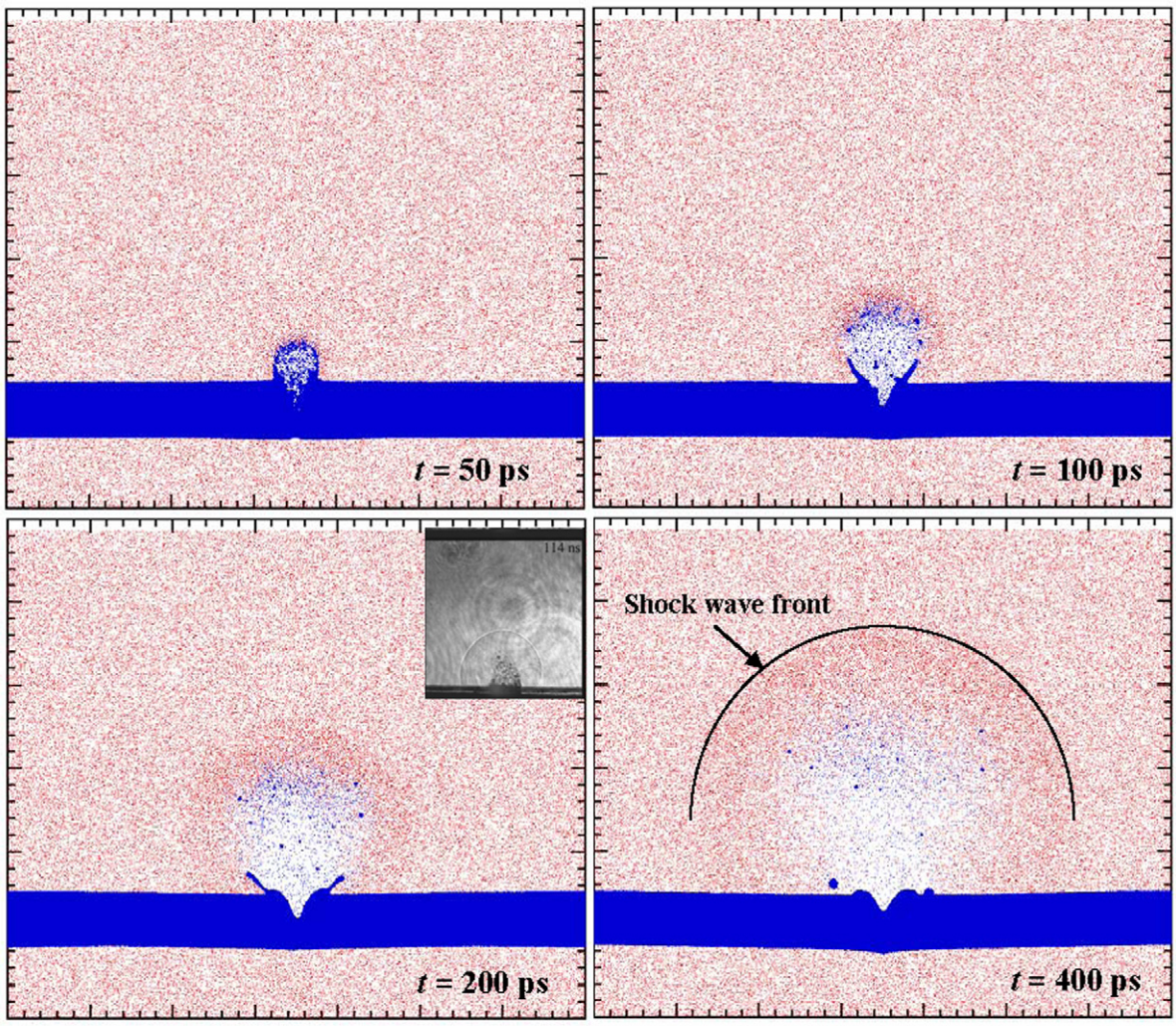

Fig. 1. (Color online.) Snapshots of atomic positions in a y (horizontal: 0–350.8 nm) – z (vertical: 0–292.3 nm) plane 1.7 nm thick centered at $x = 1.35$ nm. In this figure, the red dots denote gas atoms and the blue ones are for target atoms. The solid curve is added ($t = 400$ ps) to show the shock front. The inset in the figure at 200 ps shows the shock wave front observed in nanosecond laser–material interaction.

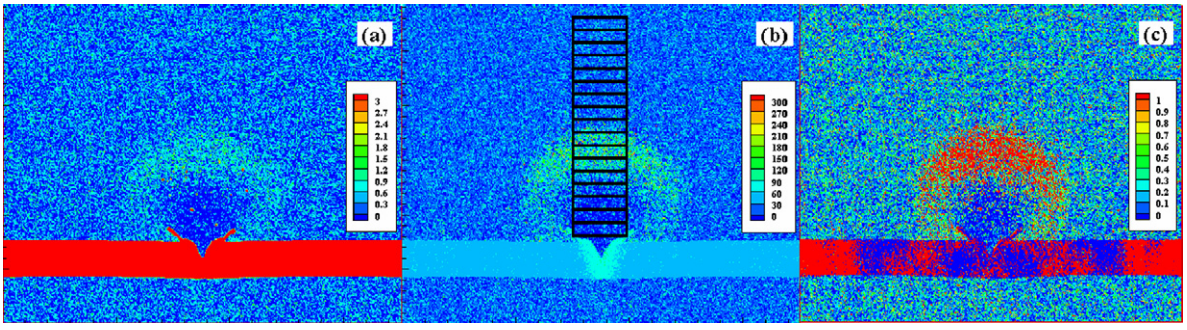

Fig. 2. Physical properties distribution of the system (200 ps) in a y (horizontal: 0–350.8 nm) – z (vertical: 0–292.3 nm) plane 1.70 nm-thick centered at $x = 1.35$ nm: (a) density (nm^{-3}), (b) temperature (K), and (c) pressure (MPa). The rectangle (not to scale) in figure (b) denotes how the cross section is divided into layers for density calculation shown in Fig. 3.

ature and pressure is averaged over a small domain of about $2.56 \times 8.52 \times 8.52$ nm^3 ($x \times y \times z$). The three properties presented in Fig. 2 are very consistent in terms of identifying the location of the shock wave. In Fig. 2(a), it is observed that in the spherical area adjacent to the surface, the gas atoms are pushed forward by moving target atoms, thus few atoms are observed here. In the shock wave region (compression region), the density is about 2 nm^{-3}, obviously higher than that in other gas regions, where the density is below 1 nm^{-3}. For the target, its density is much larger than that of the gas. Since our research focuses on the shock wave, the contour scale is adjusted to primarily demonstrate the gas region. When gas atoms are

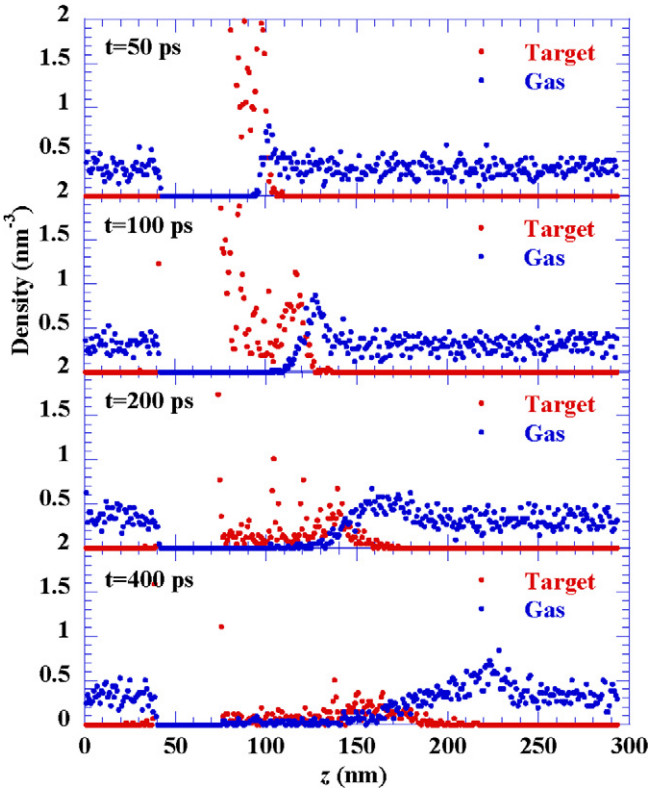

Fig. 3. Evolution of target and gas density distribution along the z direction.

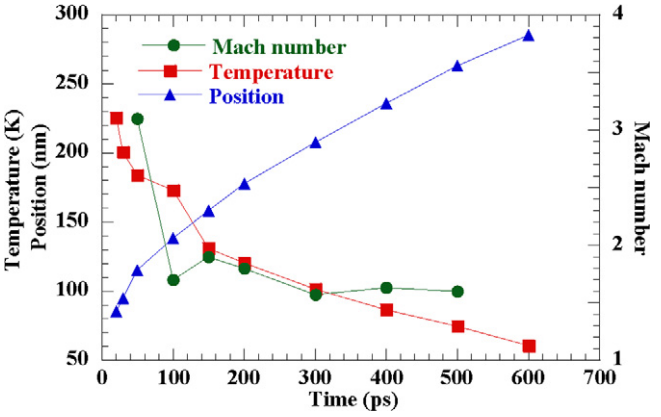

Fig. 4. Evolution of the shock wave front temperature, position and Mach number.

driven by the increasing repulsive force from the exploded target atoms, they derive high velocities that consequently lead to higher local temperatures. This is clearly observed in Fig. 2(b). In the shock wave region, the temperature of the gas is much higher due to fast compression, which is about 120 K, while the ambient temperature is only 50 K. In addition, the temperature of the top shock wave front is evidently higher than that at both sides, indicating that the shock wave is much stronger in the region directly above the laser–material interacting zone. In the compressed gas domain (shock wave) shown in Fig. 2(c), the pressure is in the order of 0.8 MPa. The highest pressure can be more than 1 MPa. This value is much larger than the pressure of the ambient gas (0.23 MPa). This sharp pressure drop from the compressed region to the ambient gas clearly demonstrates the existence of the shock wave.

In addition to the typical properties of shock waves discussed above, the evolution of gas and target/plume densities in the shock wave is also studied. This information directly reflects how the ablation plume and compressed gas penetrates into each other inside the shock wave. As shown in Fig. 2(b), a small section of several layers, the size of which is $2.56 \times 8.52 \times 0.852$ nm^3 ($x \times y \times z$), is chosen to calculate the average density for both the gas and target atoms. Fig. 3 presents the evolution of this separate layer-by-layer species density distribution at different moments. At 50 ps, the gas density is very uniform except a small peak around 100 nm. For the target part, in the range from 50 to 100 nm, its density decreases from a high level to around 0 without an evident peak in the ambient domain. At 100 ps, both the target and gas has formed an evident density peak at different locations. For the gas, the position of its peak density is about 130 nm, and still keeps propagating forward. For the target material, a clear peak forms at about 120 nm, a little behind the density peak of the background gas. Through the comparison of these two plots, it is learned that the gas atoms are pushed forward by the fast-moving target atoms. At 200 ps, both peaks keep moving forward. Because of the energy dissipation, their values become smaller in comparison with previous peaks. In the plot at 400 ps, only one evident peak (for the gas) is observed. For the target material, when the velocities of atoms are dissipated by nearby gas atoms, their movements slow down and the density is much smaller. But for the gas, a density peak still exists and keeps moving, which means the energy obtained from target atoms still pushes the gas atoms to move. With analysis of these four plots, it can be seen there is always an overlap between the two density distributions. This overlapping region is getting larger with the propagation of the shock wave. Its thickness changes from around 10 nm (at 50 ps) to more than 50 nm (at 400 ps). The mass penetration speed is estimated to be about 100 m/s.

As observed in Fig. 1, along with its propagation, the shock wave experiences a fast decay in its temperature, pressure, and velocity. This decay is calculated in great detail and shown in Fig. 4. The decay shown in Fig. 4 is for the shock wave propagating in the direction normal to the target surface. It is seen that at the beginning, the surface is under a continuous heating process, and the neighboring gas temperature is as high as 230 K. Then the shock wave propagates in the gas domain, the movement of atoms transfers energy to atoms adjacent to the shock wave. This procedure makes the shock wave temperature decrease rapidly. The more intense the movement is, the more energy is transferred. Therefore, at the beginning, the shock wave front experiences faster temperature decay than the later stage. With further propagation of the shock wave, its temperature decreases to close to 50 K, which is the initial gas temperature. From the position of the shock wave front, information can be extracted about the velocity of the shock wave. The nonlinear feature of the z–t curve indicates that the shock wave velocity decreases along the propagation. When the shock wave is referred to, one important parameter deserving

significant attention is the Mach number, which is the ratio of propagation speed to the local sound speed. During the simulation, the Mach number is always higher than 1, meaning this propagation is indeed a real shock wave. Within the first 50 picoseconds, the shock wave travels about 25 nm and its velocity is about 500 m/s. The corresponding Mach number is about 3. During the second 50 picoseconds period, the propagating distance is around 20 nm and the velocity is calculated to be 400 m/s, still making the Mach number 1.7. When the propagation continues to 500 ps, the velocity is evaluated to be about 250 m/s, still higher than local sound speed at 70 K, which is 160 m/s, and the Mach number is 1.6. From the curve, it is conclusive that the Mach number is higher than 1 all the time, meaning a nanoscale shock wave does form and propagate in laser-assisted nanomanufacturing.

4. Conclusion

In summary, MD simulation was conducted to explore the shock wave phenomena in a nanodomain during near-field laser–material interaction. The distinct generation and propagation of the shock wave was observed. During the collision of target atoms with the background gas, the strong repulsive force from the ablation plume compressed the gas atoms and formed an obvious shock wave front. The physical properties, such as density, temperature, and pressure had a very sharp change at the shock wave front. Because of energy dissipation, the temperature, pressure, and speed of the shock wave experienced a fast decay, but the Mach number always remained higher than 1, meaning the shock wave always persisted in our simulation.

Acknowledgements

Support for this work from NSF (CMS: 0457471), Nebraska Research Initiative, Air Force Office for Scientific Research and MURI from ONR is gratefully acknowledged. X. Wang also thanks the very helpful discussion with Dr. Zhaoyan Zhang at UNL.

References

[1] S. Toshiharu, N. Yoshihito, JSAP Int. 5 (2002) 22.
[2] N. Fang, H. Lee, C. Sun, X. Zhang, Science 308 (2005) 534.
[3] E.X. Jin, X.F. Xu, J. Quant. Spectrosc. Radiat. Transfer 93 (2005) 163.
[4] L. Wang, E.X. Jin, S.M. Uppuluri, X.F. Xu, Opt. Express 14 (2006) 9902.
[5] Y.F. Lu, B. Hu, Z.H. Mai, W.J. Wang, W.K. Chim, T.C. Chong, Jpn. J. Appl. Phys. 40 (2001) 4395.
[6] Y.F. Lu, Z.H. Mai, W.K. Chim, Jpn. J. Appl. Phys. 38 (1999) 5910.
[7] J. Jersch, F. Demming, K. Dickmann, Appl. Phys. A 64 (1997) 29.
[8] Y.F. Lu, Z.H. Mai, Y.W. Zheng, W.D. Song, Appl. Phys. Lett. 76 (2000) 1200.
[9] J. Jersch, K. Dickmann, Appl. Phys. Lett. 68 (1996) 868.
[10] J. Jersch, F. Demming, L.J. Hildenhagen, K. Dickmann, Appl. Phys. A 66 (1998) 29.
[11] Y.F. Lu, Z.H. Mai, G. Qiu, W.K. Chim, Appl. Phys. Lett. 75 (1999) 2359.
[12] B. Hu, Y.F. Lu, Z.H. Mai, W.D. Song, W.K. Chim, in: First International Symposium on Laser Precision Microfabrication, Omiya, Saitama, Japan, 2000, pp. 232.
[13] Z.H. Mai, Y.F. Lu, S.M. Huang, W.K. Chim, J.S. Pan, J. Vac. Sci. Technol. B 18 (2000) 1853.
[14] Z.H. Mai, Y.F. Lu, W.D. Song, W.K. Chim, Appl. Surface Sci. 154–155 (2000) 360.
[15] A. Chimmalgi, T. Choi, C.P. Grigoropoulos, in: ASME International Mechanical Engineering Congress and Exposition, New Orleans, LA, 2002, pp. 291–295.
[16] S.M. Huang, M.H. Hong, Y.F. Lu, B.S. Lukỳanchuk, W.D. Song, T.C. Chong, J. Appl. Phys. 91 (2002) 3268.
[17] S.N. Luo, D.C. Swift, T.E. Tierney IV, D.L. Paisley, G.A. Kyrala, R.P. Johnson, A.A. Hauer, O. Tschauner, P.D. Asimow, High Pressure Res. 24 (2004) 409.
[18] D. Kohen, C.C. Martens, J. Chem. Phys. 111 (1999) 4343.
[19] M. Villagrán-Muniz, H. Sobral, R. Navarro-González, Meas. Sci. Technol. 14 (2003) 614.
[20] S.H. Jeong, R. Greif, R.E. Russo, J. Phys. D: Appl. Phys. 32 (1999) 2578.
[21] X. Wang, J. Phys. D: Appl. Phys. 38 (2005) 1805.
[22] M.P. Allen, D.J. Tildesley, Computer Simulation of Liquids, Clarendon Press, Oxford, 1987.
[23] X. Wang, Y. Lu, J. Appl. Phys. 98 (2005) 114304.
[24] C. Porneala, D.A. Willis, Appl. Phys. Lett. 89 (2006) 211121.